Static and Oscillatory Tests on a Generic Combat Aircraft Model in a Low Speed Wind Tunnel

G. Guglieri *
Consiglio Nazionale delle Ricerche - Centro di Studio per la Dinamica dei Fluidi
F.B. Quagliotti †
Politecnico di Torino - Aerospace Engineering Dept.

Abstract

This experimental activity is part of a cooperative research program concerning aircraft dynamics and maneuverability, developed by AGARD FDP Working Group 16.

The static and oscillatory characteristics of a generic combat aircraft model - designed and assembled by WG16 during 1993 - were investigated in the D3M low speed wind tunnel at *Politecnico di Torino.* The experiments were performed at $\alpha = 0° \div 45°$ with different sideslip angles and airspeeds.

Pitch and roll dynamic data (direct, cross and cross-coupling derivatives) were obtained with the small oscillation amplitude technique.

The effects of some relevant configuration elements were analysed, both in static and in dynamic conditions: leading edge extensions (LEXs) and forebody strakes were adopted and the influence of transition fixing was investigated. Some of these experimental results are presented and shortly discussed, and a few relevant preliminary conclusions are given.

Nomenclature

b	Wing span (m)
c_m	Mean chord (m)
c	Mean aerodynamic chord (m)
C_l	Rolling moment coeff.
$C_{l\beta} \sin\alpha$	Rolling moment stiffness coeff.
$C_{lp} + C_{l\dot{\beta}} \sin\alpha$	Rolling moment damping coeff.
C_n	Yawing moment coeff.
$C_{n\beta} \sin\alpha$	Yawing moment stiffness coeff.
$C_{np} + C_{n\dot{\beta}} \sin\alpha$	Yawing moment damping coeff.
C_m	Pitching moment coeff.
$C_{m\alpha}$	Pitching moment stiffness coeff.
$C_{mq} + C_{m\dot{\alpha}}$	Pitching moment damping coeff.
C_Y	Lateral force coeff.
$C_{Y\beta} \sin\alpha$	Lateral force stiffness coeff.
$C_{Yp} + C_{Y\dot{\beta}} \sin\alpha$	Lateral force damping coeff.
C_Z	Normal force coeff.
$C_{Z\alpha}$	Normal force stiffness coeff.
$C_{Zq} + C_{Z\dot{\alpha}}$	Normal force damping coeff.
f	Oscillation frequency (Hz)
J_x	Roll model inertia (Kg m^2)
J_y	Pitch model inertia (Kg m^2)
k	Reduced osc. frequency ($\frac{\omega l}{2V_\infty}$)
l	Ref. length (m) [c for pitch or b for roll mode]
l_T	Length of transition strips
Ma	Mach number
Re	Reynolds number [based on c]
S	Wing area (m^2)
S_{WT}	Tunnel cross section (m^2)
TPI	Politecnico di Torino
V_∞	Airspeed (m/s)
W	Model weight (Kg)
α	Angle of attack (rad or deg)
β	Angle of sideslip (rad or deg)
δ_e	Elevator angle (deg)
ϕ	Oscillation amplitude in roll (deg)
ϕ_S	Angular position of forebody strakes (ref. to stagnation line)
ϕ_T	Angular position of transition strips (ref. to stagnation line)
ω	Oscillation frequency (rad/s)
$\overline{\sigma}$	Measurement uncertainty (%)
θ	Oscillation amplitude in pitch (deg)

Introduction

The enhancement of combat aircraft performance has led to the design of aerodynamically unstable configurations, stabilized and controlled by means of advanced fly-by-wire flight control systems, which reduce pilot workload, improving flight envelope and handling qualities. Progress in aircraft control techniques is enabling maneuvering up through extreme angles of attack. In this particular flight regime unusual combinations of angular rates and accelerations are encountered. Aicraft maneuvering at high angles of attack exhibit several possible advantages over configurations with more restricted flight envelopes. As a consequence, the capability of performing high rate maneuvers and heading reversals - even in asymmetric flight - are considered typical operational and design requirements.

*Scientist Researcher, Member AIAA
†Associate Professor, Member AIAA

Future agile aircrafts should be capable of high turning rates, increased control of acceleration and deceleration during nose-pointing maneuvers, and improved lifting characteristics.
This last requirement [1] can be obtained for conventional two-surfaces configurations at high angles of attack adopting high-lift devices on wing and leading edge extensions, the latter generating stable vortex flow over the wing up to $30° \div 35°$. Similar improvements of lift can be obtained either with conventional slender configurations with sharp-edged LEXs on the wing, or with integrated airframes, formed by a lifting surface of complex planform, which combines the fuselage nose and two engine nacelles with underwing inlets.

All of these considerations suggest that a detailed analysis of flowfield around the aircraft flying at high angle of attack is required.
The flow is separated and unsteady, with the dual impact of reducing effectiveness of conventional moving surface controls and introducing a critical sensitivity to lateral oscillations and divergence.
Instabilities related with the steady vortex pair emanating from the forebody of the aircraft may result in a destabilizing yawing moment of significant magnitude, so that the resulting moments from forebody vortex asymmetry can be larger than the restoring control power available from the rudder. Hence, in order to maintain lateral control at high angles of attack an alternative method for the generation of yawing moment is required. Several research activities [2,3] are concentrated on the development of active and passive control techniques of the forebody vortices, trying to correct aircraft instabilities by direct control of the forebody flow.
The experimental results demonstrate that the nature of the flow to be controlled and its dependence on angle of attack is complex. At moderate angles, the flow is stable and symmetric. As the angle increases, a steady asymmetry may appear in vortex positions, producing a strong yawing moment. At higher α the flow becomes unsteady, typically characterized by the alternate shedding of forebody vortices, which reduce the time averaged destabilizing yawing moment. As a consequence, the additional lateral control required should operate in regions of steady vortex asymmetry or periodic vortex shedding.

The analysis of the behaviour of forebody and wing leading edge vortices becomes even more difficult if an oscillatory motion is superimposed on a starting steady flight condition.
In these conditions, large non linear configuration dependent variations of stability derivatives with angle of attack, sideslip angle, controller deflection(s) and Mach number are detected. Large measurement uncertainties are typically observed for wind tunnel dynamic stability derivatives, due to significant aerodynamic interferences and motion frequency and amplitude effects. Finally, the influence of aerodynamic coupling ($C_{m\beta}, C_{n\alpha}$) and hysteresis ($\dot{\alpha}$ and $\dot{\beta}$ derivatives) cannot be neglected.

Wind tunnel experiments have been generally used to develop flight vehicles, but new trends in military aircraft design are placing greater demands on the capabilities of ground test facilities. The traditional dynamic simulation of maneuvering aircraft cannot be limited to the usual linearised superposition of steady state data and unsteady small disturbances. Advanced test techniques for the analysis of high amplitude maneuvers are being developed, but are not completely realized. On the other hand, the computational modeling of flight vehicles is progressing rapidly. Unfortunately, unsteady flows around maneuvering aircraft cannot be adequately predicted using present day capabilities in CFD. Therefore, integrated test and evaluation methodologies are emerging which combine ground testing, flight motion modeling and CFD.

Anyway, wind tunnel tests [4] are the primary source for dynamic stability parameters (oscillatory and rotary balance methodologies).

Conventional test methods can be considered accurate in low angle of attack flight where the aircraft aerodynamics is linear and cross-coupling and acceleration derivatives are negligible. As angle of attack increases and associated non linear flow resulting from separation and asymmetric vortex shedding occurs, secondary cross coupling and acceleration derivatives become large. Hence, using a limited aerodynamic database to predict the performance of a maneuvering aircraft in the stall and post-stall region will not model some of the most important non linear and hysteresis effects. As a matter of fact, the relative importance of cross-coupling and acceleration derivatives in modeling high $-\alpha$ aircraft motions is widely accepted [5,6,7].

With the aim of solving some of the critical aspects related with the experimental determination of a complete set of stability parameters for the simulation of high performance aircraft dynamics, AGARD Working Group 16 focused its activity on a cooperative programme, based on wind tunnel tests and detailed comparisons of data obtained in different facilities with rotary and oscillatory rigs on the same model [8,9,10,11].

Part of the contribution of *Politecnico di Torino* and some preliminary conclusions on this experimental activity are discussed in the present paper.

The Experimental Program

The wind tunnel experiments at TPI were performed, both in static and oscillatory conditions, at different angles of attack α and sideslip β.
The body axes reference system was adopted for the reduction of aerodynamic coefficients.
The configuration effects were investigated. Hence, the leading edge extensions (LEXs) were removed, the transition on the fuselage was fixed and two forebody strakes were added [9] ($\phi_S = \pm 105°$).

Config.	Transition	Lex	Forebody Strakes
BC	Free	On	Off
BNL	Free	Off	Off
BCT	Fixed	On	Off
BST	Fixed	On	On

Table 1: The model configurations tested at TPI.

α – range (deg)	β (deg)	V_∞ (m/s)	Re	Conf.
$0° \div 45°$	$0°$	25	525000	BC
$0° \div 45°$	$0°$	30	630000	BC
$0° \div 45°$	$+5°$	30	630000	BC
$0° \div 45°$	$-5°$	30	630000	BC
$0° \div 45°$	$+10°$	30	630000	BC
$0° \div 45°$	$-10°$	30	630000	BC
$0° \div 45°$	$0°$	30	630000	BC – $\delta_e = +30°$
$0° \div 45°$	$0°$	30	630000	BC – $\delta_e = -30°$
$0° \div 45°$	$0°$	40	840000	BC
$0° \div 45°$	$0°$	40	840000	BC – repeated
$0° \div 45°$	$0°$	30	630000	BNL
$25° \div 45°$	$0°$	30	630000	BC – roll mode
$25° \div 45°$	$+10°$	30	630000	BC – roll mode
$25° \div 45°$	$-10°$	30	630000	BC – roll mode
$0° \div 45°$	$0°$	30	630000	BCT
$0° \div 45°$	$+5°$	30	630000	BCT
$0° \div 45°$	$-5°$	30	630000	BCT
$0° \div 45°$	$+10°$	30	630000	BCT
$0° \div 45°$	$-10°$	30	630000	BCT
$0° \div 45°$	$0°$	40	840000	BCT
$0° \div 45°$	$0°$	30	630000	BST
$0° \div 45°$	$+5°$	30	630000	BST
$0° \div 45°$	$-5°$	30	630000	BST

Table 2: The test matrix in static conditions.

The forebody strakes were fixed using an epoxy adhesive. The transition strips were obtained using several grit disks (thickness $\approx$ 0.2 mm) bonded to the forebody by means of a thin adhesive film ($\phi_T = \pm 40°$, l_T = 400 mm from the model apex).

The airspeed range was limited to $V_\infty = 25 \div 40$ m/s.

Dynamic experiments were performed with constant oscillation frequency. The effect of amplitude was investigated for the roll mode only.

The Experimental Apparatus

The Wind Tunnel

The D3M low speed wind tunnel is a closed circuit tunnel with a contraction ratio of 5.44. The test section is circular (diameter 3 m.) and its length is 5 m.
The turbulence factor is 1.2 and the turbulence level is 0.3% with typical fundamental frequencies lower than

α – range (deg)	β (deg)	V_∞ (m/s)	f (Hz)	k	θ (deg)	Conf.
$0° \div 42.5°$	$0°$	30	2.5	0.083	$\pm 1°$	BC
$0° \div 42.5°$	$+5°$	30	2.5	0.083	$\pm 1°$	BC
$0° \div 42.5°$	$-5°$	30	2.5	0.083	$\pm 1°$	BC
$0° \div 42.5°$	$+10°$	30	2.5	0.083	$\pm 1°$	BC
$0° \div 42.5°$	$-10°$	30	2.5	0.083	$\pm 1°$	BC
$0° \div 25°$	$0°$	40	2.5	0.062	$\pm 1°$	BC
$0° \div 42.5°$	$0°$	30	2.5	0.083	$\pm 1°$	BNL
$0° \div 42.5°$	$0°$	30	2.5	0.083	$\pm 1°$	BST
$0° \div 42.5°$	$+5°$	30	2.5	0.083	$\pm 1°$	BST

Table 3: The test matrix in oscillatory conditions (pitch mode).

α – range (deg)	β (deg)	V_∞ (m/s)	f (Hz)	k	ϕ (deg)	Conf.
$0° \div 42.5°$	$0°$	30	2.5	0.180	$\pm 1°$	BC
$0° \div 42.5°$	$+5°$	30	2.5	0.180	$\pm 1°$	BC
$0° \div 42.5°$	$0°$	40	2.5	0.135	$\pm 1°$	BC
$0° \div 42.5°$	$+5°$	40	2.5	0.135	$\pm 1°$	BC
$25° \div 42.5°$	$0°$	30	2.5	0.180	$\pm 2°$	BC
$0° \div 42.5°$	$0°$	30	2.5	0.180	$\pm 1°$	BST
$0° \div 42.5°$	$+5°$	30	2.5	0.180	$\pm 1°$	BST

Table 4: The test matrix in oscillatory conditions (roll mode).

10 Hz at $V_\infty = 50$ m/s.

The Model

The model has a generic combat aircraft configuration.

The AGARD WG16-A model components were designed by IMFL and manufactured at DLR (aerodynamic surfaces), at Aermacchi (fuselage) and at DRA (horizontal tail disks). The components were assembled at TPI.

In order to support the model using the TPI vertical strut, a specific ventral door was fit to the model.

The model was statically balanced (adding a balancing weight inside of afterbody), so that the model oscillation in pitch was performed with respect to the center of gravity.

The blockage ratio between the model frontal area and the wind tunnel cross section $S_{WT} = 7.068$ m^2 was evaluated. This geometrical ratio is compatible with the α – range considered ($S/S_{WT} = 2.9\%$ at $\alpha = 45°$).

The Model Support

A specific servo-mechanical unit was adopted in order to perform static tests on the aircraft model and to generate the small amplitude harmonic motion in the two rotational degrees of freedom separately (pitch and roll), required for the application of the direct forced oscillation technique.

The facility was used at *Politecnico di Torino* in

Length	1.227 m
Fuselage diameter	0.100 m
Wing area	0.19364 m^2
Mean chord c_m	0.2784 m
Mean aerodynamic chord c	0.3168 m
Wing span b	0.6862 m
Model weight W	6.200 Kg
Model inertia J_x	$\approx$ 0.0025 Kg m^2
Model inertia J_y	$\approx$ 0.5200 Kg m^2

Table 5: The dimensions of the WG16-A model.

Coefficient	$\alpha < 20°$ (%)	$\alpha > 20°$ (%)
C_Y	$\pm$0.065	$\pm$0.426
C_Z	$\pm$0.213	$\pm$0.702
C_l	$\pm$0.244	$\pm$0.789
C_m	$\pm$0.297	$\pm$0.781
C_n	$\pm$0.028	$\pm$0.652

Table 6: The repeatability of static measurements.

the D3M low speed wind tunnel [12,13,14]. A vertical strut supports the model, that is connected to the strain gauge balance by an internal leverage, that links the fuselage with an oscillating vertical rod. The leverage configuration can be easily changed according to the different primary oscillations (pitch, roll).
The harmonic motion of the model is excited by a driving unit, that is placed under the floor of the wind tunnel test section; it is powered by a DC motor and it is linked to the main rod, that supports the fuselage by a gearbox connected to an adjustable flywheel. Setting the flywheel radius, it is possible to modify the oscillation amplitude of the model, within the limit of $\pm$ 50 mm (i.e. $\theta = \pm 3.5°$). The oscillation frequency of the model (maximum 5 Hz for lighter models) is set by the rotation speed of the DC motor.

Note that the asymmetry of the mechanichal setup has a moderate influence on stability coefficients measured at low α with sideslip angle, due to the interactions between the main rod and the model wake. This effect is negligible for $\alpha > 15°$. Correlations with previously measured derivatives on the Standard Dynamics Model are being used for the pourpose of correcting this asymmetric support interference.
The aerodynamic interference due to the roll mode setup (a second rod is present behind the model) was evaluated in static conditions [8].

The large angular motion that is necessary to modify the angles of attack and sideslip of the model, both in static and dynamic tests, is generated by two different step-motors: the former, translating vertically the dynamic motion unit, acts on the rod and it changes the main leverages position, that determine the angle of attack of the model (α ranges from $-7°$ to $+45°$); the latter rotates the vertical strut, modifying the angle of sideslip (β ranges from $-13°$ to $+13°$).

An electronic control unit is interfaced to the mechanical apparatus by a complete set of sensors, transducers and micro-switches. The power drivers of the actuators are electrically connected to the control unit, that is linked to the control PC by a special electronic device (interface board). Synchronization with the data acquisition computer is possible.

The Data Acquisition System

The aerodynamic loads acting on the model were measured with a 5 component internal strain gauge balance (axial force component was not measured). The average measurement uncertainty of the force transducer is $\overline{\sigma} = \pm 0.75$ % as a percentage of the full-scale aerodynamic loads acting on the model at $V_\infty = 40$ m/s. The balance voltage supply, the signal amplification factor and the filter settings of the conditioning unit were optimized in order to minimize the noise components. Different data acquisition units were adopted for static and oscillatory tests.

Static Force Measurements

The balance outputs were multiplexed and measured by a high precision integrating voltmeter, interfaced with the computer by a programmable simulation card. The signals were averaged over 50 samples with an integration period of 20 ms. The repeatability of two series of static data was evaluated as a percentage of data range ($V_\infty = 40$ m/s, $\beta = 0°$).

Dynamic Force Measurements

The signals were measured with a high speed 12 bit analog-to-digital converter. Parallel sampling was obtained with a specific sample-and-hold unit. The balance outputs were sampled at 512 samples/s/channel for a period of 10 s. The coefficients were averaged over a number of six periods (i.e. 60 s) and the repeatability of these six measurements was evaluated as a percentage of data range for the pitch mode only ($V_\infty = 30$ m/s, $\beta = 0°$, k = 0.083, $\theta = \pm 1°$).

The software elaboration is based on Fourier analysis, as in-phase and out-of-phase load components are evaluated for wind-on/off conditions.

The Experimental Results.

Static and oscillatory results obtained at TPI will be presented in order to discuss the aerodynamic be-

Test condition	Static derivatives	Dynamic derivatives
Pitch mode	$C_{Z\alpha}$	$C_{Zq} + C_{Z\dot{\alpha}}$
	$C_{m\alpha}$	$C_{mq} + C_{m\dot{\alpha}}$
	$C_{Y\alpha}$	$C_{Yq} + C_{Y\dot{\alpha}}$
	$C_{l\alpha}$	$C_{lq} + C_{l\dot{\alpha}}$
	$C_{n\alpha}$	$C_{nq} + C_{n\dot{\alpha}}$
Roll mode	$C_{Y\beta} \sin\alpha$	$C_{Yp} + C_{Y\dot{\beta}} \sin\alpha$
	$C_{l\beta} \sin\alpha$	$C_{lp} + C_{l\dot{\beta}} \sin\alpha$
	$C_{n\beta} \sin\alpha$	$C_{np} + C_{n\dot{\beta}} \sin\alpha$
	$C_{Z\beta} \sin\alpha$	$C_{Zp} + C_{Z\dot{\beta}} \sin\alpha$
	$C_{m\beta} \sin\alpha$	$C_{mp} + C_{m\dot{\beta}} \sin\alpha$

Table 7: The dynamic derivatives measured at TPI.

Coefficient	$\alpha < 20°$ (%)	$\alpha > 20°$ (%)
$C_{Z\alpha}$	± 0.973	± 2.663
$C_{m\alpha}$	± 1.188	± 4.884
$C_{Zq} + C_{Z\dot{\alpha}}$	± 0.766	± 2.032
$C_{mq} + C_{m\dot{\alpha}}$	± 1.010	± 3.561

Table 8: The repeatability of dynamic measurements.

haviour of the AGARD WG16-A model.

Static coefficients

The normal force and pitching moment coefficients are strongly affected by the contribution of leading edge vortices. In particular, when LEXs are removed, a sharp reduction (25%) of maximum C_Z is observed (see Fig. 3). The lift increment due to leading edge extensions is clearly evident for $\alpha > 10°$, where vortex induced suction effects on wing upper surface generate a relevant percentage of total normal force. The trend of pitching moment (see Fig. 4) is stabilized for $\alpha = 15° \div 30°$ by LEX removal, as a consequence of the combined shift of aerodynamic center location and lift reduction.

A marginal influence on lateral force coefficient of transition fixing and forebody strakes is found at lower angles of attack (see Fig. 5). On the contrary, the strong asymmetries detected for $\alpha = 25° \div 45°$ on the basic configuration BC are significantly reduced, even if the stabilizing contribution of transition strips is moderate and limited only to the higher α – range.
Longitudinal coefficients are not changed by the addition of forebody strakes, but the suppression of destabilizing vortex asymmetries is evident, confirming the opportunity of further experimental investigation concerning the optimization of the geometry of this efficient vortex control device.

The onset of forebody vortex asymmetry (see Fig. 6) can be identified at $\alpha = 22°$, where C_n starts to increase, reaching a maximum at $\alpha \approx 42°$. The yawing moment coefficient is obviously reduced to lower values when transition is fixed and forebody strakes are added.

Both C_Y and C_n for BST configuration continue to increase moderately at higher incidence ($\alpha > 40°$), as a possible consequence of leading edge vortex burst asymmetries.

The deflection of horizontal stabilizer generates a linear increment of normal force and pitching moment for $\alpha < 20°$, while the effect of δ_e becomes non linear at higher angles of attack.

Dynamic coefficients

The consequences of configuration changes on longitudinal stability parameters are given in Fig. 9,10,11 and 12. The $C_{m\alpha}$ derivative is fairly insensitive to LEXs removal for $\alpha < 10°$. On the contrary, at higher incidence the basic configuration BC remains in the positive unstable range, while BNL is characterized by negative values, confirming the static trend of C_m coefficient.
An intermediate behaviour is found by fixing transition and adding forebody strakes: for $\alpha < 25°$ the $C_{m\alpha}$ derivative for BST configuration matches with BC, while at higher angles of attack it gets closer to BNL stable values.

Leading edge extensions produce an evident increment of normal force derivative at intermediate angles of attack.
The trend for BST configuration is comparable with BC only for $\alpha < 15°$. High angle of attack strakes effects on $C_{Z\alpha}$ are related with the remarkable changes in vortex symmetry induced on the forebody.

A comment concerning model setup effects for $C_{mq} + C_{m\dot{\alpha}}$ derivative is difficult, even if this derivative has a stable non linear trend for the three configurations considered.

Similar considerations apply for $C_{Zq} + C_{Z\dot{\alpha}}$. Note that a sharp increase of normal force damping is observed at $\alpha \approx 30°$ for the basic configuration.

In Fig. 13,14 and 15 the static derivatives obtained with roll experiments are presented.
Some differences are found between the BC and the BST configuration. At high angles of attack the trend of $C_{Y\beta} \sin\alpha$ coefficient is smoothed when forebody strakes are added, even if an opposite variation with α is found when a comparison is made with the basic configuration. The strakes (BST) reduce the non linearities versus α of $C_{l\beta} \sin\alpha$, but no direct relationship with forebody vortex asymmetries can be established.
On the contrary, an evident increase of directional stability ($C_{n\beta} \sin\alpha$) is observed at high angles of attack, due to the reduction of sidewash induced by vortex asymmetries on vertical stabilizer.

Roll damping derivatives are shown in Fig. 16,17 and 18. The trend of these stability parameters is typically a non linear function of angle of attack.
Lateral force and yawing moment derivatives become unstable at high α, but the magnitude of the destabilizing peak at $\alpha = 40°$ is smoothed for the straked model. Differently, the negative stability margin for

$C_{lp} + C_{l\dot{\beta}} \sin\alpha$ is reduced for BST configuration.

Finally, the increment of ϕ (see Fig. 19,20) is too small to generate any significant change of stability parameters in the high angle of attack range. The local linearity assumption for the model aerodynamic behaviour still applies.

Concluding Remarks

The tests performed [8,9,10,11] on AGARD WG16 model are giving interesting informations concerning configuration effects on wind tunnel stability parameters measured with different techniques adopted in several laboratories.

The contribution of *Politecnico di Torino* has been shortly discussed.

At conclusion of Working Group 16 activity a complete set of data will be collected and refined, in order to establish some of the aerodynamic requirements of future high performance aircrafts, identifying a possible strategy for the efficient mathematical modeling of high angle of attack maneuvers.

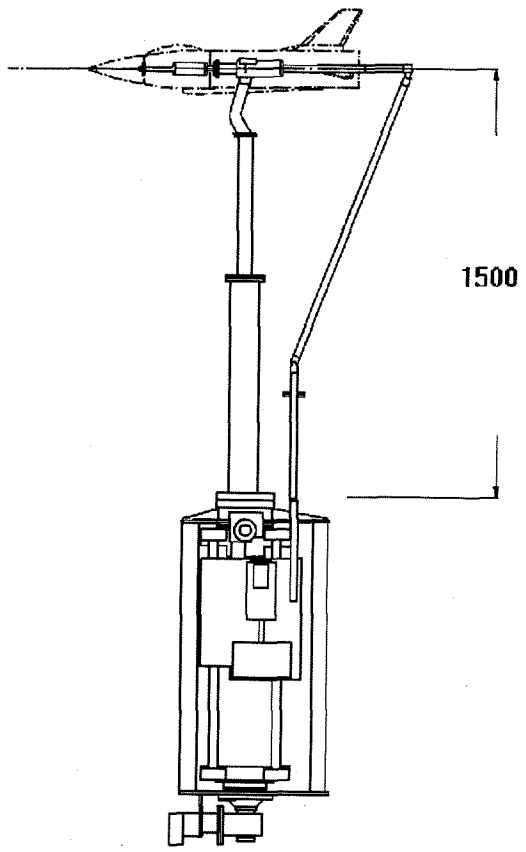

Fig. 1. The experimental apparatus.

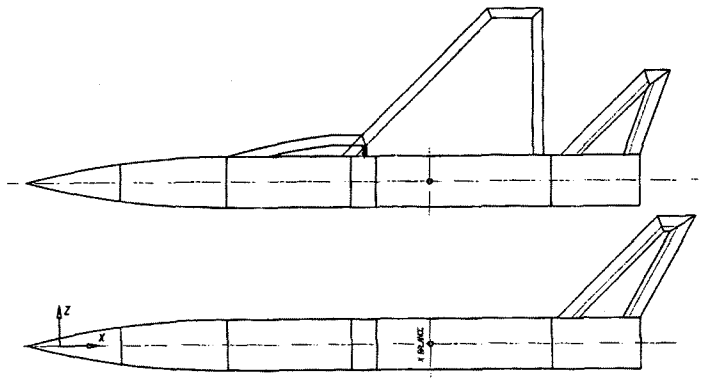

Fig. 2. The AGARD WG16-A model.

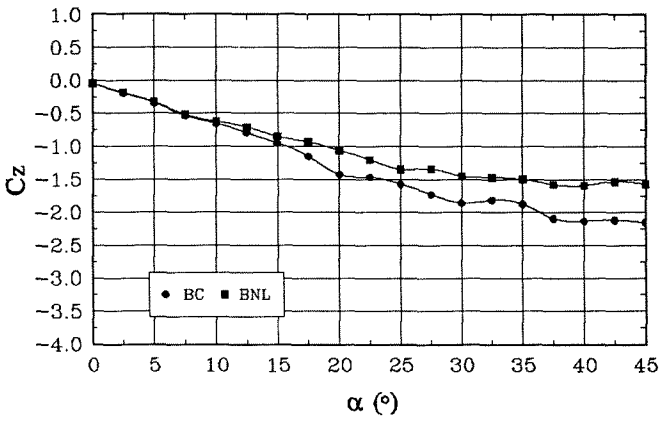

Fig. 3. The effect of configuration on C_Z.

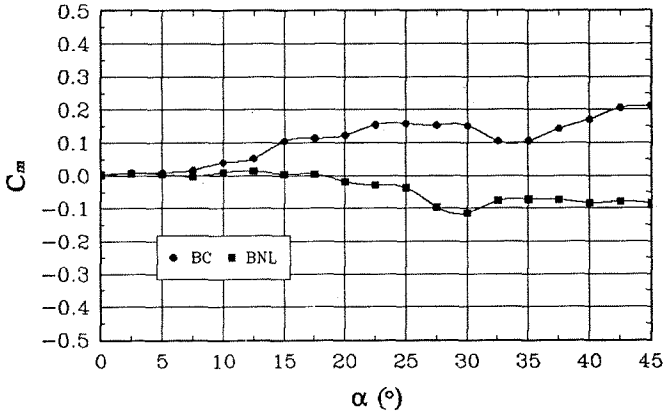

Fig. 4. The effect of configuration on C_m.

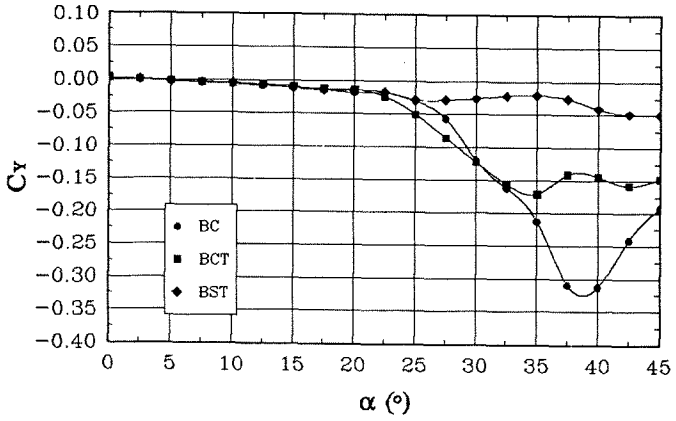

Fig. 5. The effect of configuration on C_Y.

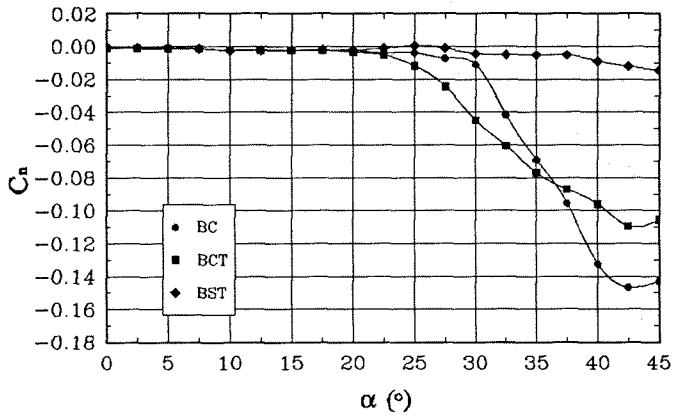

Fig. 6. The effect of configuration on C_n.

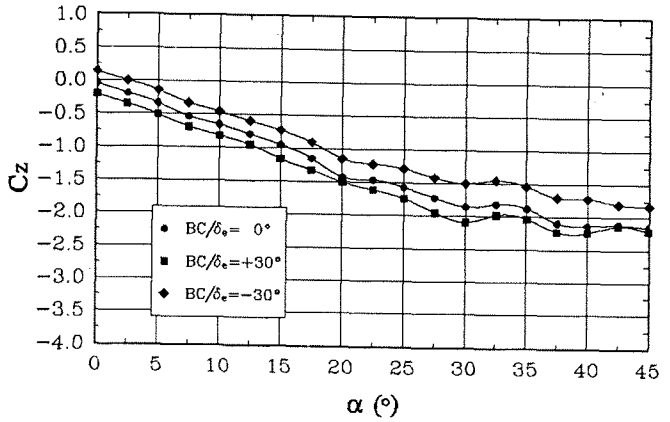

Fig. 7. The effect of tail deflection on C_Z.

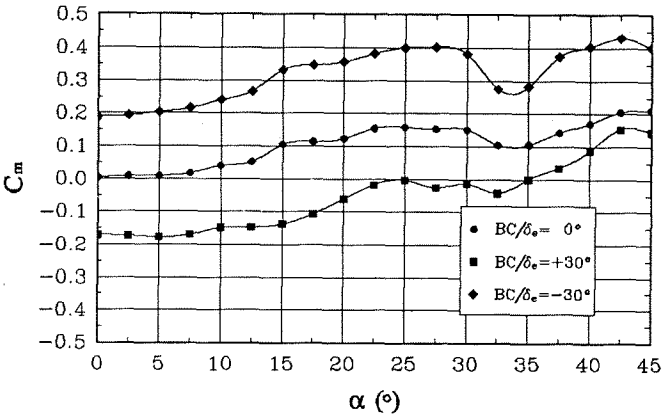

Fig. 8. The effect of tail deflection on C_m.

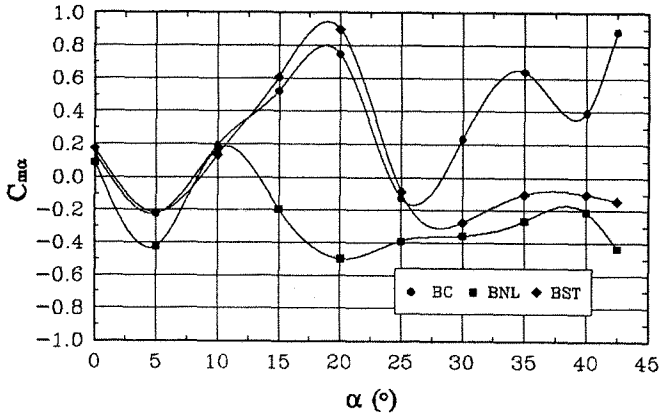

Fig. 9. The effect of configuration on C_{m_α}.

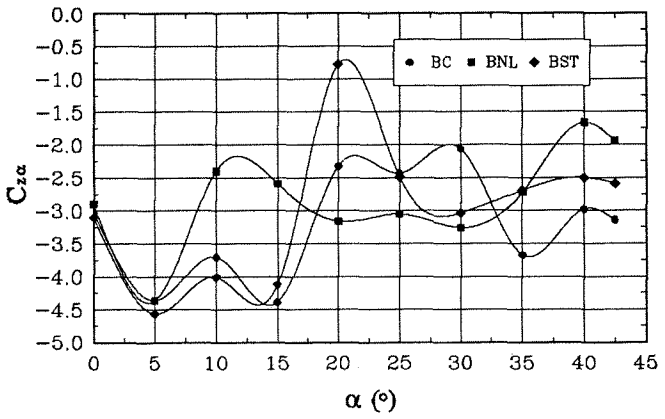

Fig. 10. The effect of configuration on C_{Z_α}.

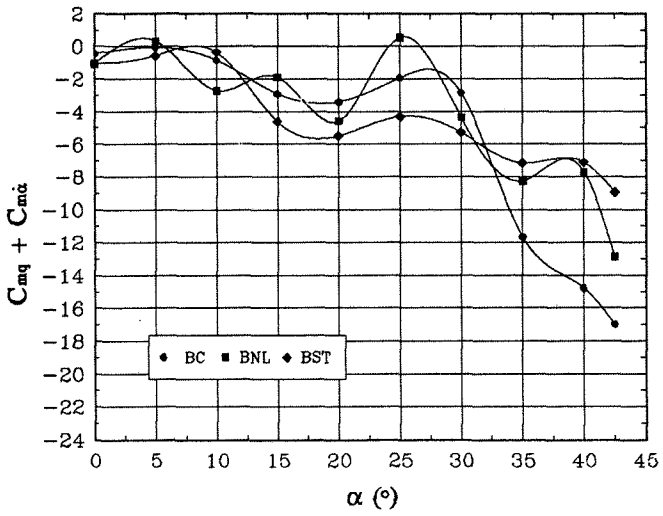

Fig. 11. The effect of configuration on $C_{mq} + C_{m_{\dot{\alpha}}}$.

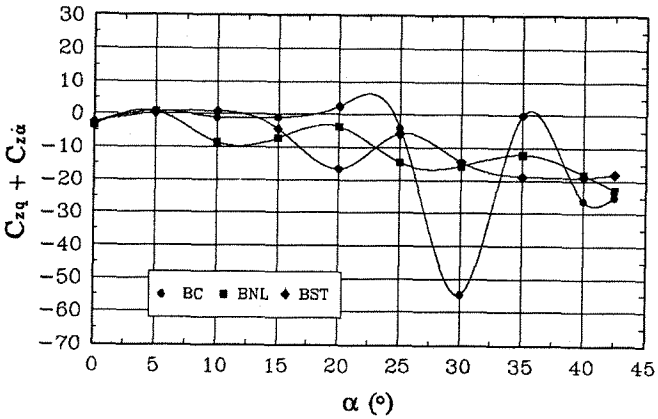

Fig. 12. The effect of configuration on $C_{Zq} + C_{Z_{\dot{\alpha}}}$.

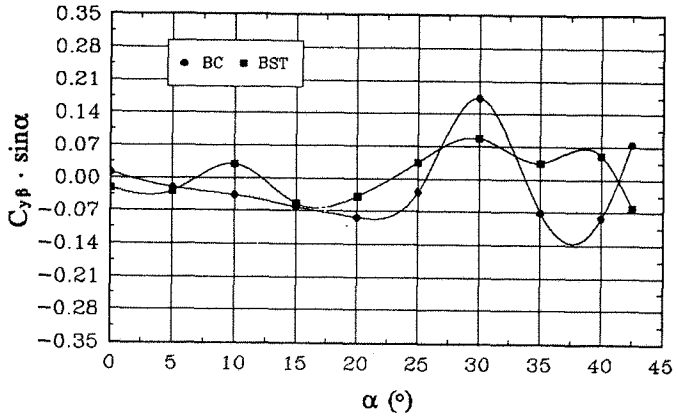

Fig. 13. The effect of configuration on C_{Y_β}.

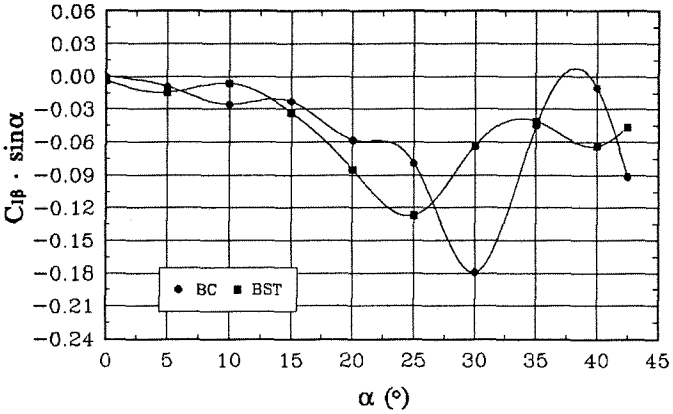

Fig. 14. The effect of configuration on C_{l_β}.

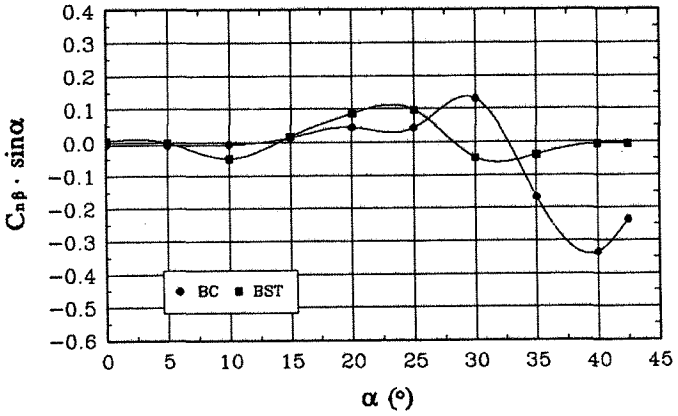

Fig. 15. The effect of configuration on $C_{n\beta}$.

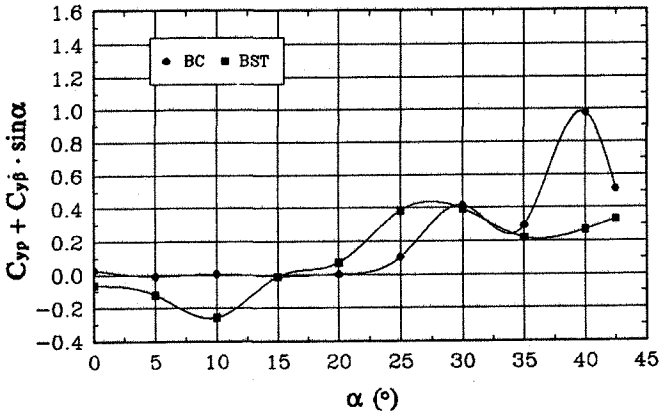

Fig. 16. The effect of configuration on $C_{Yp} + C_{Y\dot{\beta}} \sin\alpha$.

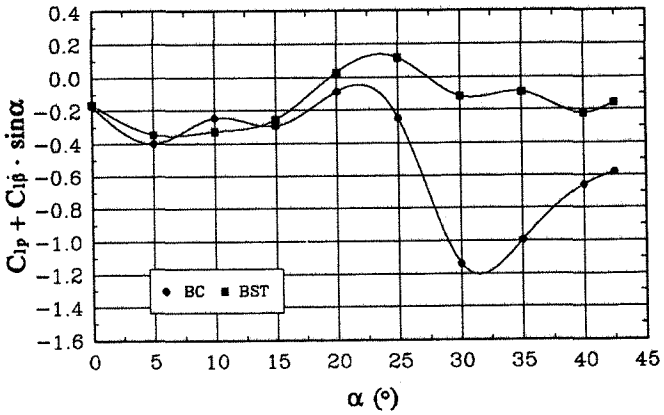

Fig. 17. The effect of configuration on $C_{lp} + C_{l\dot{\beta}} \sin\alpha$.

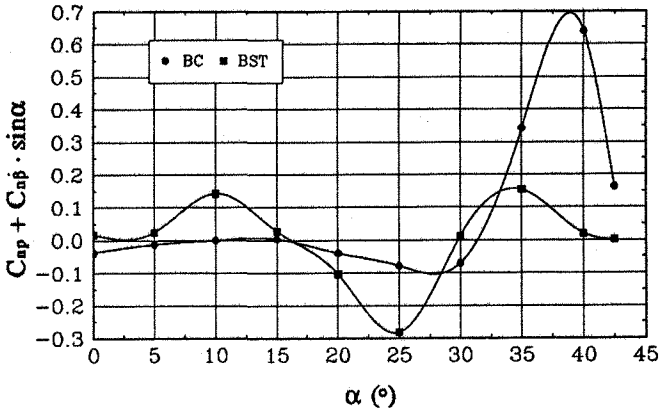

Fig. 18. The effect of configuration on $C_{np} + C_{n\dot{\beta}} \sin\alpha$.

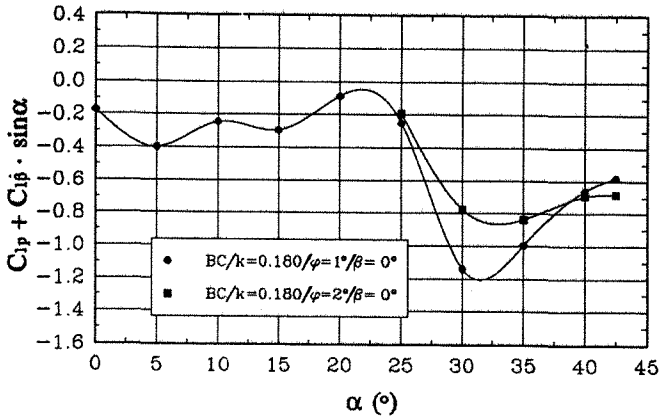

Fig. 19. The effect of oscillation amplitude on $C_{lp} + C_{l\dot{\beta}} \sin\alpha$.

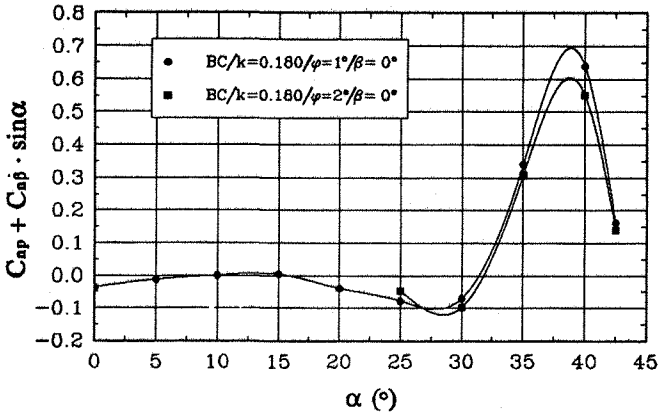

Fig. 20. The effect of oscillation amplitude on $C_{np} + C_{n\dot{\beta}} \sin\alpha$.

References

[1] Irodov, R.D., Petrov, A.V.,
Aerodynamic Design of Supermaneuverable Aircraft , AGARD CP-548, 1993.

[2] Malcolm, G.N.,
Forebody Vortex Control , Progress in Aerospace Sciences, vol. 28, n. 3, 1991.

[3] Wood, N.J., Crowther, W.J.,
Yaw Control by Tangential Forebody Blowing , AGARD CP-548, 1993.

[4] Orlik-Rueckemann, K.J. (Course Director),
Special Course on Aircraft Dynamics at High Angles of Attack , AGARD R-776, 1991.

[5] Orlik-Rueckemann, K.J.,
Aerodynamic Aspects of Aircraft Dynamics at High Angles of Attack , J. of Aircraft, vol. 20, n. 9, 1983.

[6] Orlik-Rueckemann, K.J.,
Sensitivity of Aircraft Motion to Cross-Coupling and Acceleration Derivatives , AGARD LS-114, 1981.

[7] Tobak, M., Schiff, L.B.,
Aerodynamic Mathematical Modelling - Basic Concepts, AGARD LS-114, 1981.

[8] Guglieri, G., Quagliotti, F.,
Static and Oscillatory Tests on a Generic Combat Aircraft Model in a Low Speed Wind Tunnel , TPI TN-75/93, 1993.

[9] O'Leary, C.O., Weir, B., Walker, J.M.,
Preliminary Results from Tests on Model WG16B at DRA Bedford , DRA Preliminary Report, 1993.

[10] Pertile, R.,
AGARD WG16 Reference Models: Static and Rotary Balance Tests in Aermacchi Wind Tunnel, Aermacchi Rep. 567-ANG-292 A, 1993.

[11] Tristrant, D.R., Gauthier, F.F., Vanmansart, M.G.,
Dynamic Tests in ONERA IMFLille Wind Tunnels with AGARD Generic Fighter Model , IMFL TN 94113, 1994.

[12] Guglieri, G., Quagliotti, F.,
Determination of Dynamic Stability Parameters in Low Speed Wind Tunnel , 9TH AIAA Applied Aerodynamics Conference, Baltimore, U.S.A., 1991.

[13] Guglieri, G., Quagliotti, F.,
Wind Tunnel Experimental Investigation of a High Performance Aircraft Model , The Aeronautical Journal, vol. 97, pp. 73-80, 1993.

[14] Fusco, F., Guglieri, G.,
Experimental Investigation on Aircraft Dynamic Stability Parameters , Meccanica, vol. 28, pp. 61-68, 1993.